NANO LETTERS

pubs.acs.org/NanoLett

# High-Efficiency Ordered Silicon Nano-Conical-Frustum Array Solar Cells by Self-Powered Parallel Electron Lithography

**Yuerui Lu and Amit Lal***

School of Electrical and Computer Engineering, Cornell University, Ithaca, New York 14853, United States

**ABSTRACT** Nanostructured silicon thin film solar cells are promising, due to the strongly enhanced light trapping, high carrier collection efficiency, and potential low cost. Ordered nanostructure arrays, with large-area controllable spacing, orientation, and size, are critical for reliable light-trapping and high-efficiency solar cells. Available top-down lithography approaches to fabricate large-area ordered nanostructure arrays are challenging due to the requirement of both high lithography resolution and high throughput. Here, a novel ordered silicon nano-conical-frustum array structure, exhibiting an impressive absorbance of ∼99% (upper bound) over wavelengths 400−1100 nm by a thickness of only 5 $\mu$m, is realized by our recently reported technique self-powered parallel electron lithography that has high-throughput and sub-35-nm high resolution. Moreover, high-efficiency (up to 10.8%) solar cells are demonstrated, using these ordered ultrathin silicon nano-conical-frustum arrays. These related fabrication techniques can also be transferred to low-cost substrate solar energy harvesting device applications.

**KEYWORDS** Solar cell, photonic crystal, nanocone, parallel lithography, light trapping

Solar cells with Si nanowire (Si NW) arrays incorporating radial p−n junctions not only have antireflective, broad band optical absorption properties but also offer the advantage of orthogonalizing the light absorption and carrier collection processes, which is the challenging problem for bulk Si solar cells.[1−13] Previously, single Si NW radial p−n junction solar cells, using vapor−liquid−solid NW growth, were reported.[14] This single NW solar cell had a low open circuit voltage ($V_{oc}$), possibly due to the p−i−n structure, resulting in low overall solar cell efficiency of less than 3.4%. Large-area solar cells based on Si NW were reported using Au catalytic chemical vapor deposited (CVD) p-type Si NW, followed with a plasma-enhanced CVD conformal n-type amorphous silicon (a-Si:H) layer to create the photoactive p−n junction.[15] These solar cells showed very low conversion efficiency (∼0.1%), particularly due to the geometry of the NWs with random and uncontrolled NW orientation and varied NW diameter distribution. Recently, large-area solar cells from arrays of silicon NW with radial p−n junctions were shown,[16,17] using an aqueous suspension of silica beads to get a close-packed monolayer, followed by deep reactive ion etching to form NW and boron diffusion to form the radial p−n junction. By reducing surface roughness and improving the NW diameter and density control, the solar cell efficiency was enhanced significantly from initially 0.5% to as high as 5.3%. But its overall efficiency is still not high for practical application, probably due to the imperfect NW spacing, and absence of any surface passivation.

Calculations have showed that with optimized wire spacing, diameter, and wire height, vertical Si NW array solar cells with photonic crystal architecture could offer conversion efficiency as high as 24% or more,[18] due to photonic crystal optical absorption enhancement effect with the presence of optical guided resonance modes.[18−21] Moreover, theoretical study also shows that ordered Si NW structures with small variations in the radius of the wires could create additional resonant modes at other frequencies not present in the perfectly ordered structures, leading to broad band solar-energy harvesting.[21] Amorphous silicon nanocone arrays were demonstrated to have enhanced optical absorption in the 400−700 nm wavelength range,[2] but they are hard to apply to high-performance thin film solar cells due to the random nanocone spacing and wide cone size distribution.

The fabrication of large-area ordered controllable Si nanostructure arrays needs top-down planar lithography with both high throughput and high resolution. Conventional optical lithography has high throughput, but its critical dimension (CD) is limited to a fraction of the wavelength.[22] Traditional electron beam lithography (EBL) has the highest resolution <10 nm, but EBL suffers from high cost and low throughput due to the required electron beam raster scanning serial exposure.[23] Nanoimprint lithography could be used to achieve nanostructured arrays, but the prospect of mask mechanical contact to substrate leads to a large number of defects and short mask life.[24] Our recently reported technique self-powered parallel electron lithography (SPEL),[25,26] using large-area planar radioactive $\beta$-elec-

---

* Correspondence to, amit.lal@cornell.edu.

**Received for review: 08/13/2010**
**Published on Web: 10/12/2010**

© 2010 American Chemical Society

DOI: 10.1021/nl102867a | *Nano Lett.* **2010,** *10,* 4651–4656

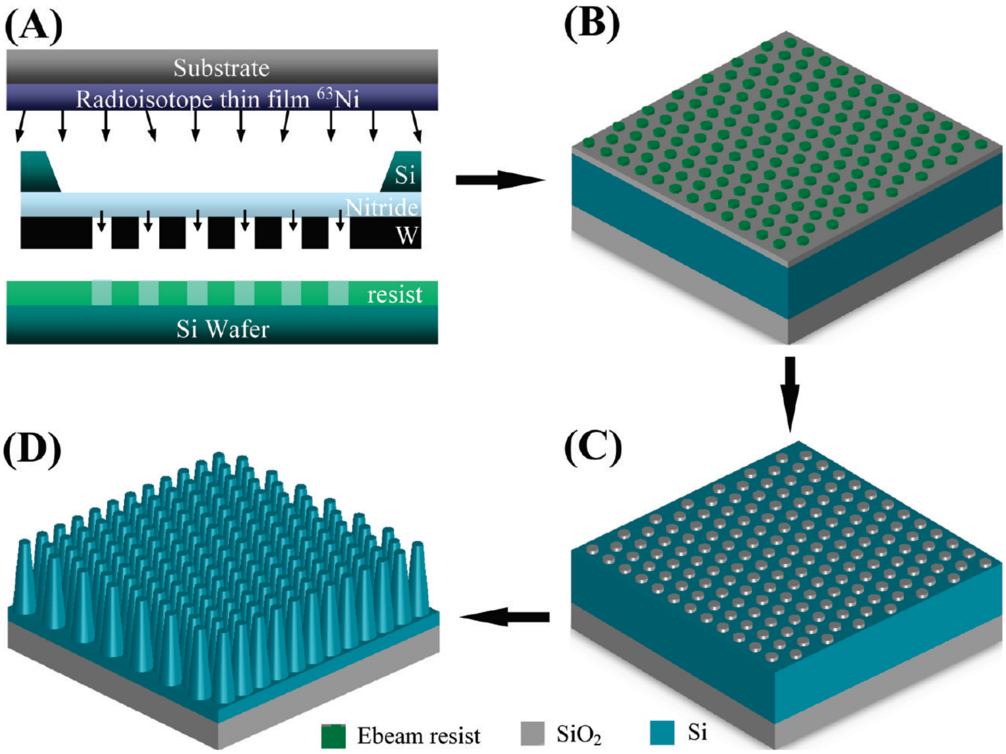

**FIGURE 1.** Schematic drawings for ordered Si NCF arrays, fabricated by SPEL. (A) Cross section schematic drawing for SPEL experimental setting up, using large-area planar radioactive $\beta$-electron thin film emitters (top) to parallel expose e-beam resist (bottom) through a stencil mask (middle). Using nature's high-energy particle, SPEL potentially enables large-area massively parallel high throughput electron lithography with low cost, while maintaining sub-35-nm resolution. (B) Ebeam resist is patterned on stack substrate SiO$_2$(0.2 $\mu$m)/Si(5 $\mu$m)/SiO$_2$(2 $\mu$m)/Si, by SPEL. (C) Pattern is transferred to SiO$_2$ layer by oxide RIE etching, using ebeam resist as the etching mask. (D) Ordered Si NCF arrays are formed by Si RIE etching, using SiO$_2$ as the etching mask. The bottom Si substrate of the SOI wafer is not shown here.

tron thin film emitters to parallel expose e-beam resist through a stencil mask, demonstrated sub-35-nm resolution. Using naturally emitted high-energy beta particles, the SPEL system can be compact as the electron focusing column needed in EBL systems is no longer needed. Elimination of vacuum in SPEL will significantly simplify the overall lithography system and greatly reduce the cost, while enabling large area massively parallel high-throughput electron lithography with high resolution. Here, we successfully used SPEL to fabricate a novel ordered Si nano-conical-frustum (NCF) array structure, which exhibits an impressive absorbance of ~99% (upper bound) over wavelengths 400−1100 nm with a thickness of only 5 $\mu$m. Moreover, high-efficiency (up to 10.8%) solar cells have been demonstrated, by using these ordered Si NCF arrays.

Figure 1 shows the schematic illumination of the fabrication processes for ordered NCF arrays. A thin layer of plasma-enhanced chemical vapor deposition (PECVD) silicon dioxide (200 nm thick) was deposited on a silicon on insulator (SOI) (Si (5 $\mu$m)/SiO$_2$ (2 $\mu$m)/Si stack) wafer substrate. SPEL was used to pattern the e-beam resist, and the pattern was transferred to SiO$_2$, using SiO$_2$ reactive ion etching (RIE). Ordered Si NCF arrays were formed, using a silicon angled RIE etching recipe, with SiO$_2$ as the etching mask.

Ordered Si NCF arrays with different slant angles can be obtained, depending on the reactive ion etching conditions (Supporting Information). Figure 2 shows the scanning electron microscopy (SEM) images of two types of NCF arrays, with different slant angles, using the same ordered SiO$_2$ post arrays as the etching mask. The first NCF arrays (Figure 2A,B) have 170 nm of top radius ($r_1$), 400 nm of base radius ($r_2$), 3.5 $\mu$m of height ($h$), 3.8° of slant angle ($\theta$), and 800 nm of lattice constant. The second (Figure 2C,D) type have 170 nm of equal top and base radii, height of 3.5 $\mu$m, 0° slant angle, and 800 nm lattice constant, which we name ordered quasi-nanowire (QNW) arrays. In experiments, the top radii and the lattice constant were controlled by SPEL mask design. The slant angle and height are determined by the silicon RIE etching condition and etching time, respectively. The bases of all the adjacent NCFs were connected (Figure 2B right), while the bases of the adjacent QNWs were apart from each other (Figure 2D).

The transmitted diffraction pattern of the ordered Si NCF arrays (800 nm lattice constant) using $\lambda = 609$ nm laser (Figure 3A), shows the high periodicity and uniformity of the nanostructures. The reflection and transmission spectra are shown in parts C and D of Figure 3, respectively. In order to get the membrane window for transmission measurements, the SOI wafer was backside etched through, by Si deep

© 2010 American Chemical Society

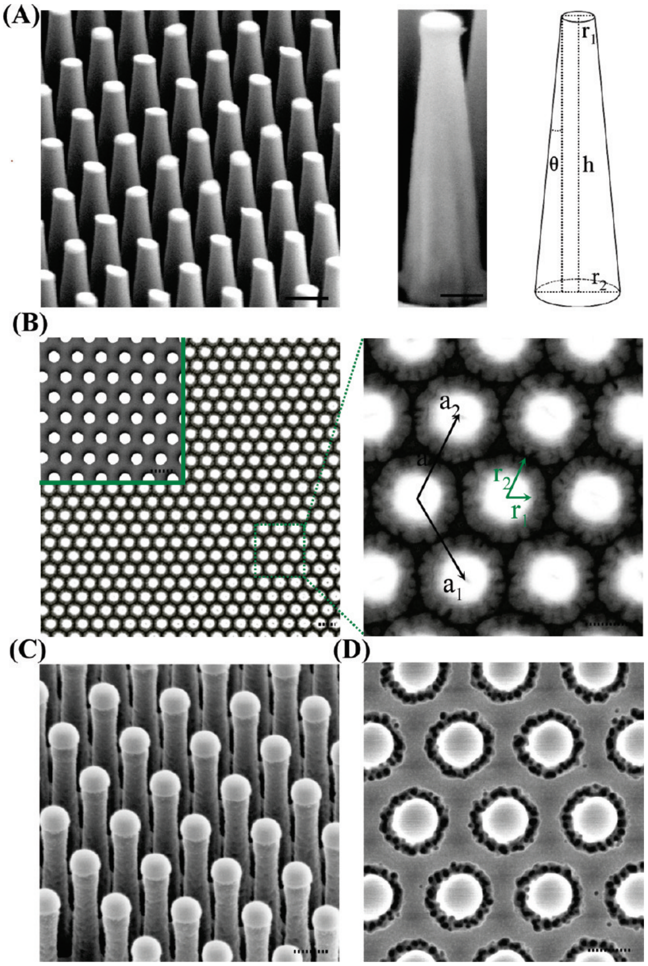

FIGURE 2. **Microscopy images of ordered Si NCF arrays and the ordered quasi-nanowire (QNW) arrays. (A) Left part shows the side view (45°) SEM image of the ordered Si NCF arrays, with scale bar 800 nm. The zoom in SEM image (45° side view) of a single NCF is shown on right, with 170 nm of top radius ($r_1$), 400 nm of base radius ($r_2$), 3.5 $\mu$m of height ($h$), and 3.8° of slant angle ($\theta$). The scale bar is 400 nm. (B) Top view SEM images of the ordered Si NCF arrays (left, 800 nm scale bar) and the zoom in SEM image (right, 400 nm scale bar). Inset shows the SEM image of the corresponding etching mask $SiO_2$ post arrays (800 nm scale bar). $a_1$ and $a_2$ are the lattice vectors, with lattice constant $a$. The bases of the adjacent NCFs are connected, with 800 nm of lattice constant and 400 nm of NCF base radius. (C) Side view (45°) SEM image of the ordered Si QNW arrays, with scale bar 400 nm. (D) Top view SEM image of the ordered Si QNW arrays in (C), with scale bar 400 nm.**

reactive ion etching (DRIE), using 4 $\mu$m of PECVD $SiO_2$ as the etching mask and the buried oxide (2 $\mu$m) as an etch stop. The window membranes consist of 3.5 $\mu$m of ordered Si NCF arrays (or QNW arrays), 1.5 $\mu$m of planar Si layer underneath and 2 $\mu$m of the SOI buried oxide. The control sample made of bare silicon membrane has a thickness of 5 $\mu$m planar Si and 2 $\mu$m of the SOI buried oxide. We obtained absorption ($A$) spectra (Figure 3E) after acquisition of reflection ($R$) and transmission ($T$) spectra, by $A = 100\% - R - T$. The ordered Si NCF arrays exhibit maximal absorbance of ~99% (upper bound) over wavelengths 400−1100 nm. A small part of diffusely reflected light was not included in the reflection measurements, due to the experimental setup limitation. Therefore, the absorption spectra represent an upper limit. Figure 4C shows relative improvements in absorption throughout the spectral range, for bare silicon (5 $\mu$m thick) and the ordered Si NCF arrays with 800 nm lattice constant. The improvement increases at longer wavelengths, where the silicon absorption decreases and the effect of light trapping increases. The improvement reaches an impressive value of 10−19 times at the 1000−1100 nm region, where silicon has very weak absorption.

In order to investigate the light trapping properties as a function of lattice constants, we fabricated three kinds of ordered NCF arrays with the same height (3.5 $\mu$m) and constant slant angle ($\theta = 3.8°$), but with different lattice constants, 600 nm ($r_1 = 69$ nm, $r_2 = 300$ nm), 800 nm ($r_1 = 170$ nm, $r_2 = 400$ nm), and 1000 nm ($r_1 = 273$ nm, $r_2 = 500$ nm) on the same SOI wafer. The reflectance spectra are shown in Figure S2A (Supporting Information). The ordered NCF arrays with 600 nm lattice constant give the lowest reflectance (<0.5%), due to the smallest top radius for minimal reflectance, which is consistent with expectations from theoretical predictions. All these three NCF samples show strong antireflective properties throughout the spectral range, which are consistent with the "black surface" (Figure 3B). Both the ordered NCF arrays with lattice constants of 800 nm and of 1000 nm show ultralow transmittance spectra (Figure S3B in the Supporting Information) throughout the spectral range 400−1100 nm, while the ordered NCF arrays with 600 nm lattice constant show slightly increasing transmittance for the wavelength near the band gap region 800−1100 nm.

Due to the maximal absorption throughout the spectra range, the ordered Si NCF arrays with 800 nm lattice constant were selected for solar cells fabrication, to see the solar energy conversion efficiency. The radial p−n junction was formed via boron ion implantation ($E = 10$ keV), starting with $n^+$-type ordered Si NCF arrays fabricated using SOI top silicon (resistivity 0.015 $\Omega \cdot$cm, doping concentration $2 \times 10^{18}$ cm$^{-3}$). Ion implantation offers the advantage of precise control over the total dose of dopants, depth profile, and most importantly works well also for high doping levels of the order of $10^{19}$−$10^{21}$ cm$^{-3}$. Considering the slant angle (3.8°) of the NCF, the sidewall implantation depth was estimated to be 20 nm, using the lateral straggling depth value calculated from SRIM ion implantation simulator. The initial doping concentration on the NCF sidewall surface was controlled to be $1 \times 10^{20}$ cm$^{-3}$ during the ion implantation. Rapid thermal annealing (RTA) at 900 °C for 60 s was used directly after implantation to activate the dopants and remove the implantation damage. In order to minimize the loss from the surface recombination coming from the large total surface area increased by NCF array geometry, a thin layer (~20 nm thick) of $SiO_2$ wet oxide was formed as the outside passivation layer for the p−n junction, at 900 °C for

© 2010 American Chemical Society

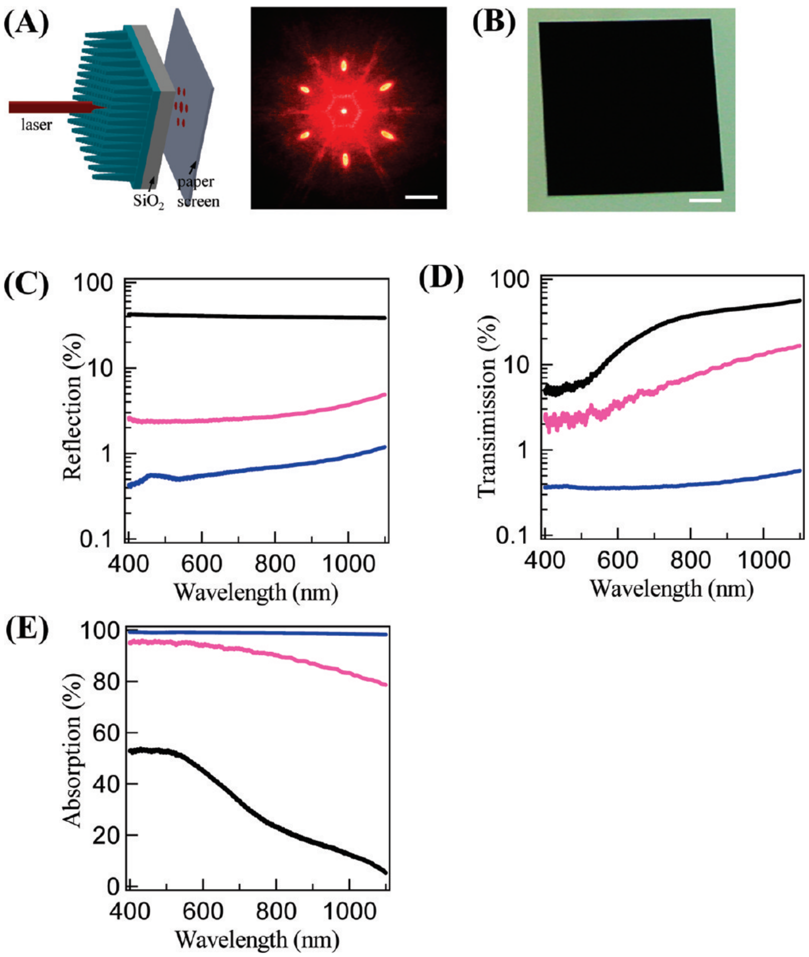

**FIGURE 3. Light trapping measurements. (A) Transmitted diffraction pattern of the NCF arrays (800 nm lattice constant) using a $\lambda = 609$ nm laser, projected onto a white paper screen and taken by digital camera. The paper screen is 4 mm away from the $SiO_2$ substrate. Scale bar is 3 mm. The window membranes consist of 3.5 $\mu$m of ordered Si NCF arrays, 1.5 $\mu$m of planar Si layer underneath and 2 $\mu$m of the SOI buried oxide. (B) Photograph of the ordered Si NCF arrays, with scale bar 1 mm. Parts C, D, and E show the measured reflection, transmission, and absorption spectra, respectively, for light normally incident on the ordered Si NCF arrays (blue), ordered Si QNW arrays (pink), and control bare silicon (black). The window membranes consist of 3.5 $\mu$m of ordered Si NCF (or QNW) arrays, 1.5 $\mu$m of planar Si layer underneath and 2 $\mu$m of the SOI buried oxide. The control bare silicon has a thickness of 5 $\mu$m.**

6 min. During the RTA and wet oxidation high temperature processes, the boron dopants diffused toward the core by approximately 80 nm more, estimated from literature,[27,28] offering a final junction depth of 100 nm and final boron doping concentration of $2 \times 10^{19}$ $cm^{-3}$ after the diffusion. From outer surface to the core center, the radial p−n junction consists of 20 nm of outside passivation $SiO_2$, 100 nm of quasi-neutral boron-doped $p^+$ type shell region, 25 nm of depletion intershell region, and 45 nm top radius (275 nm base radius) of quasi-neutral $n^+$ type Si core region (in radii). It is important to use both heavily doped $n^+$ and $p^+$ quasi-neutral region to make a small depletion region in each NCF, so that the NCF is not fully depleted, since the quasi-neutral core region should exist to conduct carriers down to the bottom contact. The schematic solar cell structure plot is shown in Figure 4A.

Figure 4B shows representative current density versus voltage measurements of the individual solar cells, under AM 1.5G normal illumination of 100 mW/$cm^2$ at room temperature. For the solar cells with only controlled bare Si and with ordered Si NCF arrays (800 nm lattice constant), they had short circuit current densities ($J_{sc}$) of 13.6 and 26.4 mA/$cm^2$, open circuit voltages ($V_{oc}$) of 0.54 and 0.59 V, fill factors (FF) of 0.71 and 0.69, and efficiencies ($\eta$) of 5.2 and 10.8%, respectively. The high energy conversion efficiency of the ordered Si NCF arrays is due to the strong light trapping and absorption properties throughout the spectra range, with the presence of both photonic crystal enhancement effect and radii-variation-induced broad band absorption. Although these NCF structure arrays have high light absorption efficiency, the solar cell efficiency is still less than half of that for bulk crystalline Si solar cells[29] and the open circuit voltage and fill factor are lower too. This is probably due to the high surface recombination losses, which are introduced by the highly enhanced surface area from the nanostructures, although a thin passivation oxide layer was used.

In summary, a novel large-area ordered silicon NCF array structure, exhibiting an impressive absorbance of ~99%

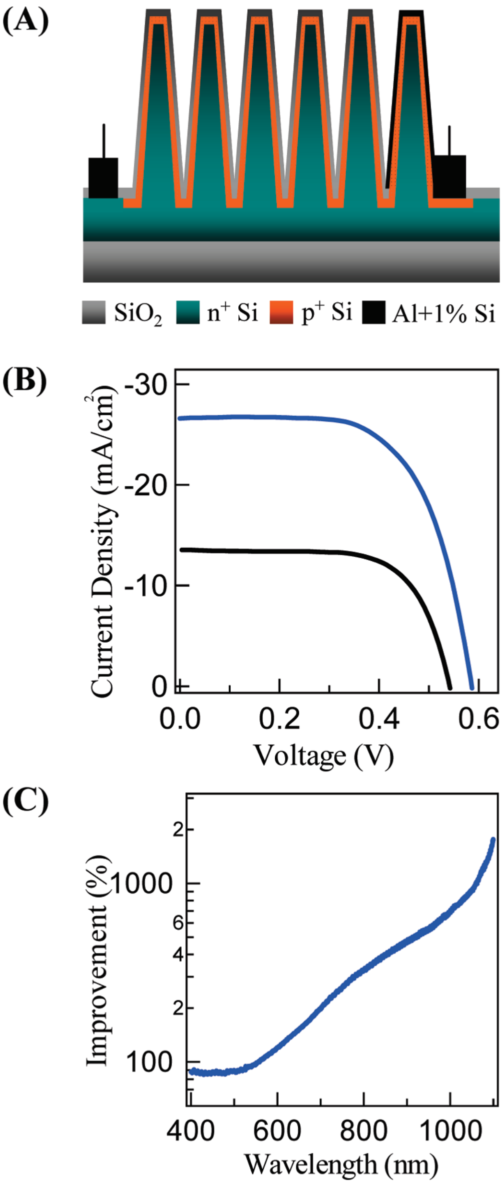

**FIGURE 4. Solar cell output characteristics. (A) Cross section schematic drawing of the solar cell structures. (B) *Current density* vs *voltage* curves for the solar cells consisting of bare silicon (black), Si NCF arrays with 800 nm (blue), under AM 1.5G normal illumination. (C) Spectrally resolved improvements in absorption for silicon NCF arrays with 800 nm lattice constant compared to that for bare silicon. The improvements are defined as the difference between values measured with ordered Si NCF arrays and those with bare silicon, divided by the value for bare silicon.**

(upper bound) over wavelengths 400−1100 nm with a thickness of only 5 $\mu$m, is demonstrated by using the SPEL technique that has the potential for very high lithography throughput, high resolution, and low cost. High-efficiency solar cells have been achieved using these ordered Si NCF arrays. Moreover, this novel high light-trapping structure array and the SPEL fabrication technique can be also used for low-cost substrate solar cells, using polysilicon or other semiconductors.[5]

**Acknowledgment.** We thank S. Tin, K. Amponsah, Z. Yu, and X. Li for discussions. Thanks to the Tobias Hanrath Laboratory for the AM1.5 measurement setup. We acknowledge support from Defense Advanced Research Projects Agency (DARPA) Microsystems Technology Office (MTO).

### *Notes*

**Competing Financial Interests.** The authors declare that they have no competing financial interests.

**Author Contributions.** All authors contributed to the scientific design, discussions and paper writing.

**Supporting Information Available.** Experimental details. This material is available free of charge via the Internet at http://pubs.acs.org.

## REFERENCES AND NOTES

(1) Huang, Y. F.; et al. Improved broadband and quasiomnidirectional anti-reflection properties with biomimetic silicon nanostructures. *Nat. Nanotechnol.* **2007**, *2*, 770–774.
(2) Zhu, J.; et al. Optical absorption enhancement in amorphous silicon nanowire and nanocone arrays. *Nano Lett.* **2009**, *9*, 279–282.
(3) Tsakalakos, L.; et al. Strong broadband optical absorption in silicon nanowire films. *J. Nanophotonics* **2007**, *1*, 013552.
(4) Fan, Z.; et al. Three-dimensional nanopillar-array photovoltaics on low-cost and flexible substrates. *Nat. Mater.* **2009**, *8*, 648–653.
(5) Fan, Z.; et al. Challenges and prospects of nanopillar-based solar cells. *Nano Res.* **2008**, *2*, 829–843.
(6) Peng, K.; et al. Aligned single-crystalline Si nanowire arrays for photovoltaic applications. *Small* **2005**, *1*, 1062–1067.
(7) Stelzner, T.; et al. Silicon nanowire-based solar cells. *Nanotechnology* **2008**, *19*, 295203.
(8) Sivakov, V.; et al. Silicon nanowire-based solar cells on glass: Synthesis, optical properties, and cell parameters. *Nano Lett.* **2009**, *9*, 1549–1554.
(9) Muskens, O. L.; Rivas, J. G. m.; Algra, R. E.; Bakkers, E. P. A. M.; Lagendijk, A. Design of light scattering in nanowire materials for photovoltaic applications. *Nano Lett.* **2008**, *8*, 2638–2642.
(10) Zhu, J.; Hsu, C. M.; Yu, Z.; Fan, S.; Cui, Y. Nanodome Solar Cells with Efficient Light Management and Self-Cleaning. *Nano Lett.* **2010**, *10*, 1979–1984.
(11) Law, M.; Greene, L. E.; Johnson, J.; Saykally, C. R.; Yang, P. D. Nanowire dye-sensitized solar cells. *Nat. Mater.* **2005**, *4*, 455–459.
(12) Michael, D.; et al. Enhanced absorption and carrier collection in Si wire arrays for photovoltaic applications. *Nat. Mater.* **2010**, *9*, 239–244.
(13) Kayes, B. M.; Atwater, H. A.; Lewis, N. S. Comparison of the device physics principles of planar and radial pn junction nanorod solar cells. *J. Appl. Phys.* **2005**, *97*, 114302–114311.
(14) Tian, B.; et al. Coaxial silicon nanowires as solar cells and nanoelectronic power sources. *Nature* **2007**, *449*, 885.
(15) Tsakalakos, L.; et al. Silicon nanowire solar cells. *Appl. Phys. Lett.* **2007**, *91*, 233117.
(16) Garnett, E.; Yang, P. D. Silicon nanowire radial p-n junction solar cells. *J. Am. Chem. Soc.* **2008**, *130*, 9224–9225.
(17) Garnett, E.; Yang, P. D. Light Trapping in Silicon Nanowire Solar Cells. *Nano Lett.* **2010**, *10*, 1082–1087.
(18) Lin, C.; Povinelli, M. L. Optical absorption enhancement in silicon nanowire arrays with a large lattice constant for photovoltaic applications. *Opt. Express* **2009**, *17*, 19371–19381.
(19) Hu, L.; Chen, G. Analysis of optical absorption in silicon nanowire arrays for photovoltaic applications. *Nano Lett.* **2007**, *7*, 3249–3252.
(20) Yu, Z.; Raman, A. & Fan, S. Fundamental Limit of Nanophotonic Light-Trapping in Solar Cells. In *Optics for Solar Energy, OSA Technical Digest (CD)*; Optical Society of America: 2010; paper PDSWB1.

(21) Chutinan, A.; John, S. Light trapping and absorption optimization in certain thin-film photonic crystal architectures. *Phys. Rev. A* **2008**, *78*, 023825.

(22) Sewell, H.; Mulkens, J. Materials for optical lithography tool application. *Annu. Rev. Mater. Res.* **2009**, *39*, 127–153.

(23) Vieu, C.; et al. Electron beam lithography: resolution limits and applications. *Appl. Surf. Sci.* **2000**, *164*, 111–117.

(24) Costner, E. A.; Lin, M. W.; Jen, W. L.; Willson, C. G. Nanoimprint lithography materials development for semiconductor device fabrication. *Annu. Rev. Mater. Res.* **2009**, *39*, 155–180.

(25) Lu, Y. R.; Lal, A. Vacuum-Free Self-Powered Parallel Electron Lithography with Sub-35-nm Resolution. *Nano Lett.* **2010**, *10*, 2197–2201.

(26) Lu, Y. R.; Yoshimizu, N.; Lal, A. Self-powered near field electron lithography. *J. Vac. Sci. Technol. B.* **2009**, *27*, 2537–2541.

(27) Plummer, J. D.; Deal, M. D.; Griffin, P. B. *Silicon VLSI Technology: Fundamentals, Practice, and Modeling*; Prentice Hall: Upper Saddle River, NJ, 2000.

(28) Garnett, E. C.; et al. Dopant profiling and surface analysis of silicon nanowires using capacitance-voltage measurements. *Nat. Nanotechnol.* **2009**, *4*, 311–314.

(29) Zhao, J.; Wang, A.; Altermatt, P.; Green, M. A. Twenty-four percent efficient silicon solar cells with double layer antireflection coatings and reduced resistance loss. *Appl. Phys. Lett.* **1995**, *66* (26), 3636–3638.

© 2010 American Chemical Society

# Supporting Information

# High-efficiency Ordered Silicon Nano-Conical-Frustum Array Solar Cells by Self-powered Parallel Electron Lithography

Yuerui Lu, Amit Lal

School of Electrical and Computer Engineering, Cornell University

## Experiment Details.

### a. Resist exposure and development for SPEL

The anisole diluted chemical amplified negative-tone e-beam resist NEB31A (Zeon Corporation) was spun on substrate in a thickness of ~ 200 nm, followed by post bake at 115 °C for 2 minutes. Then SPEL mask was put on top of the NEB31A film and the $^{63}$Ni thin film source was placed on top of the mask to expose the resist in air for 48 hours continuously (Fig.1A). The exposure was conducted in dark room due to the high sensitivity of NEB31A resist to white light. After exposure, we baked the wafer at 95 °C for two minutes, developed it in MF321 for 30 seconds, followed by DI water rinsing and nitrogen gun blow drying. The long exposure time 48 hours is needed to get enough dosage for NEB31A resist, due to the low activity of our proof-of-concept demonstration source (10 pA/cm$^2$, measured under high vacuum). We could increase the total thickness of the thin film $^{63}$Ni source to get higher total source activity so that we could get higher electron flux current density and reduce the exposure time to what we want.

### b. SPEL mask fabrication

A layer of low stress silicon nitride ($Si_3N_4$) film (~1500 nm) was deposited on both sides of a double polished silicon wafer by Low Pressure Chemical Vapor Deposition (LPCVD) at 800 °C. Then a thin layer of tungsten (300 nm thick) was sputtered on top of the bottom nitride film, followed by 20 nm of Cr evaporation on top of tungsten. Then the Cr film will be patterned by EBL (100 keV beam energy) using ZEP520 resist. Cr was etched by Cr RIE etching, using ZEP520 as the etching mask. Then tungsten was etched by tungsten RIE ($CF_4/SF_6$) etching, using Cr as etching mask. Afterwards, back-side-alignment optical lithography was used to pattern a resist window on back side of the wafer, followed by nitride RIE etching through the nitride film on the backside. Then KOH etching at 80 $^{o}$C temperature was used to back etch through the silicon wafer, stopping at the bottom nitride layer (Fig.S1).

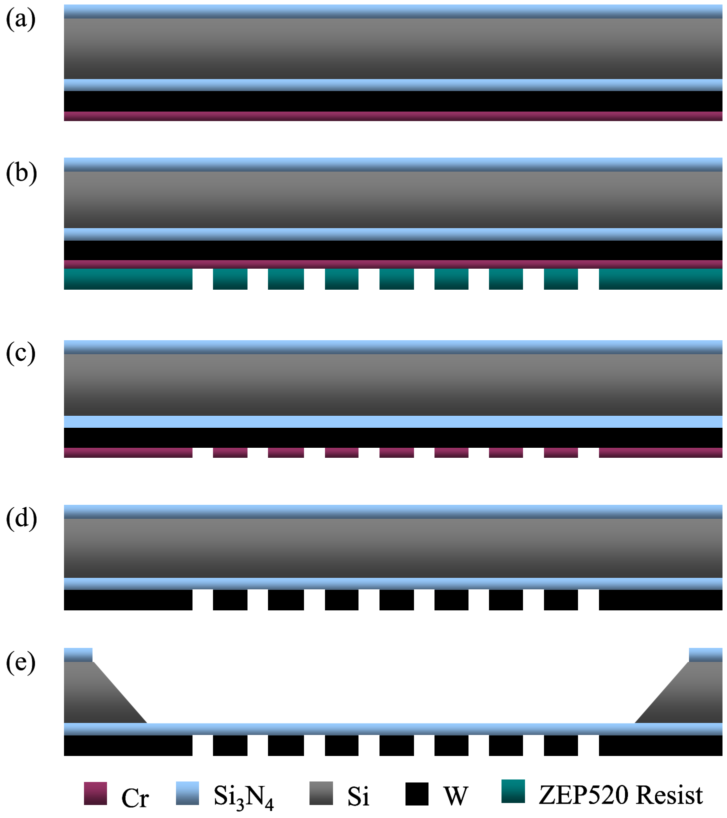

**Figure S1.** SPEL mask fabrication process. (a) Low stress LPCVD nitride (1500 nm) deposition on double polished Si (100) wafer, followed by 300 nm of W sputtering and

20 nm of Cr evaporation on the front side. (b) E-beam patterning, using ZEP520 resist. (c) Cr RIE etching, using ZEP520 as the etching mask. (d) W RIE ($CF_4/SF_6$) etching, using Cr as etching mask. (e) Back side nitride window patterning by optical lithography, nitride RIE etching, followed by KOH (80 $^{o}C$) Si etching to etch through the Si wafer.

### c. $^{63}$Ni thin film emitter

Radioactive isotopes $^{63}$Ni thin film emitter has 100.1 years long half-life, and suitable beta electron energy range ($E_{av}$ = 14.9 keV, $E_{max}$ = 67 keV). It is safe, since the low-energy beta electrons from $^{63}$Ni source can be shielded by thin layers (~ 25 μm) of most materials and could not penetrate the death skin of the human beings. The beta emitter has high stability, since the beta emission is independent of pressure or temperature.

### d. Si membrane window formation on SOI wafer

When the ordered Si NCF arrays were formed on top side of the SOI wafer, the top side was coated with a thick layer of photo resist (SPR 220-7.0, ~10 μm) to protect the NCF arrays for followed backside processes. A thick layer of PECVD $SiO_2$ (4 μm thick, at 400$^{o}$C for 20 mins) was deposited on the backside of the SOI wafer. EV620 contact aligner backside photolithography was used to open a photo resist window on the backside, followed by 20 seconds of oxygen plasma treatment to remove the resist residue after development. $SiO_2$ RIE was used to etch the 4 μm PECVD oxide. Then SOI wafer was etched through, using Si deep reactive ion etching (DRIE) ($SF_6$, for around 200mins) with the buried oxide as an etch stop. Finally, the front side photo resist protection layer was removed by acetone and followed by 20 seconds of oxygen treatment to remove the resist residue.

### e. Optical measurements

Both reflectance spectra and transmittance spectra measurements were conducted, using a xenon lamp combined with a monochromator. A small part of diffusely reflected light was not included in the reflection measurements, due to the experimental setup limitation. Therefore, the absorption spectra represent an upper limit. The solar cells were characterized at 298±2 K under AM1.5G solar simulator.

### f. RIE etching conditions for NCF arrays and QNW arrays

We could modify the RIE etching condition to adjust the slant angle of the NCF. For our NCF arrays (slant angle 3.8 degree), we used Si RIE etching condition: 70 sccm of $BCl_3$, 2 sccm of $H_2$, 20 mTorr pressure, with 65 W power. For our QNW arrays (slant angle zero degree), we used Si RIE etching condition: 70 sccm of $BCl_3$, 2 sccm of $H_2$, 10mTorr pressure, with 70 W power.

### g. Ordered Si NCF array solar cells fabrication by SPEL

200nm of PECVD $SiO_2$ was deposited at temperature 400$^oC$ onto n-type SOI wafer (Si(5μm)/$SiO_2$(2μm)/Si stack), with top Si heavily doped (resistivity 0.015 Ω·cm, doping concentration $2x10^{18}cm^{-3}$). A thin layer (~200nm thick) of negative tone chemical amplified e-beam resist NEB31A was spun on top, which was patterned by SPEL exposure using $^{63}Ni$ thin film source, followed by normal NEB31A development. $SiO_2$ ordered post arrays were formed by silicon dioxide reactive ion etching (RIE), using NEB31A as the etching mask. Ordered Si NCF arrays were created by angled Si RIE etching (70 sccm of $BCl_3$, 2 sccm of $H_2$, 20 mTorr, and 15 mins), using $SiO_2$ as the etching mask. After RIE, the top $SiO_2$ bead mask was removed in buffered oxide etcher (BOE) 6:1 solution for 10 minutes. Photo resist SPR 220-4.5 layer was spun on top (3000

RPM for 60 seconds, ~5 μm thick, post bake 115 °C for 2 mins) and followed by photolithography to open the window, defining the key area that needs ion implantation. After development, oxygen plasma was used for 20 seconds to remove the resist residue in the resist window. Then boron ion implantation at energy of 10 keV, with substrate rotated, was used to form the radial p-n junction on each single NCF. Considering the slant angle (3.8 degree) of the NCF arrays, the sidewall surface implantation depth of the NCF was estimated to be 20nm, using the lateral straggling depth value calculated from SRIM ion implantation simulator. The initial doping concentration on the NCF sidewall surface was controlled to be $1x10^{20}$ $cm^{-3}$ after the ion implantation. For the sidewall of the NCF, the effective doping is highly reduced, compared with that for planar surface, due to the small slant angle and the highly enhanced total surface area of the NCF structure (enhanced factor F, ~15). Therefore, in order to achieve enough sidewall doping concentration, the total doping dosage used should time a factor of F. After ion implantation, the SPR 220-4.5 resist was removed by acetone. Rapid thermal annealing (RTA) at 900 °C for 60 seconds was used to activate the dopants and remove the implantation damage. In order to minimize the loss from the surface recombination due to the large total surface area increased by NCF array geometry, a thin layer (~ 20 nm thick) of $SiO_2$ wet oxide was formed as the outside passivation layer for the p-n junction, at 900 degree for 6 minutes. Photolithography was used to pattern the top finger grid electrodes and the back contact electrodes, followed by silicon oxide RIE etching process to remove the thin $SiO_2$ passivation layer (~20 nm). Al + 1% Si alloy metal were sputtered for the top and back contacts, followed by lift off and annealing at 400°C in nitrogen for 30 minutes to get ohmic contact.

### h. Light trapping for NCF arrays with different lattice constants.

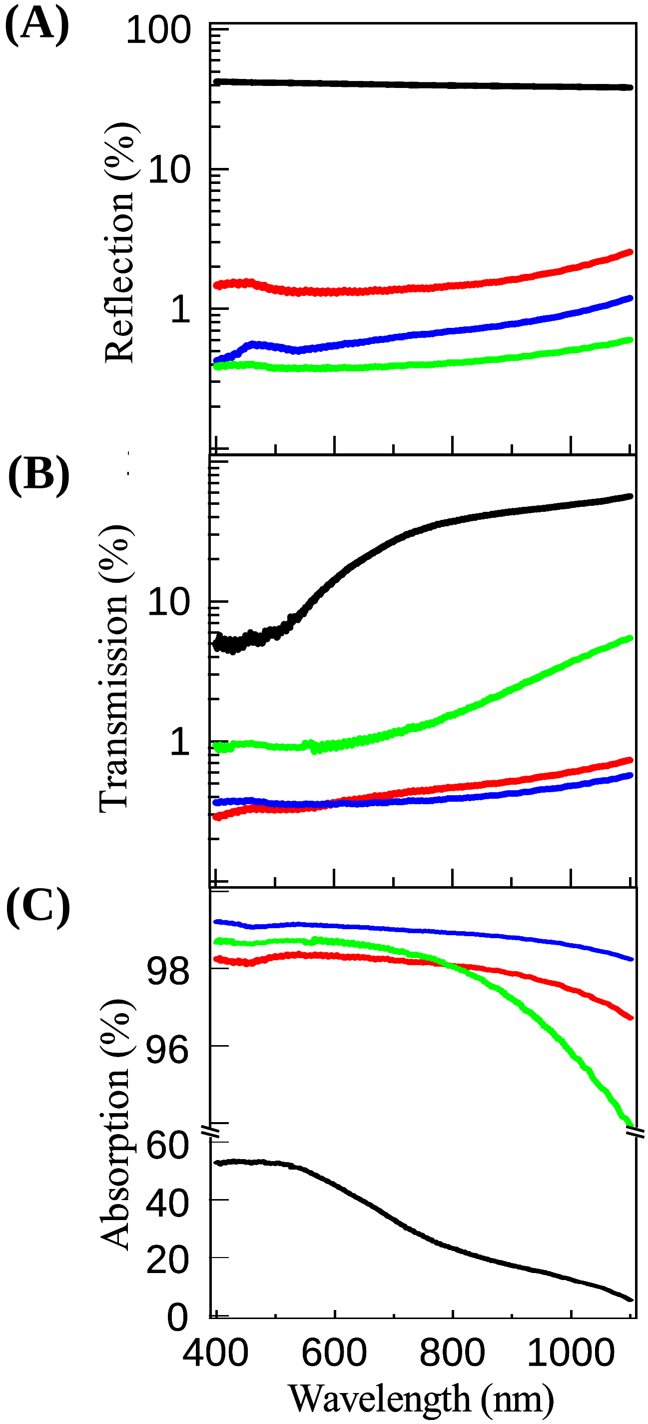

**Figure S2.** Experimentally measured reflection (A), transmission (B) and absorption (C) spectra for light normally incident on the ordered Si NCF arrays. Four types of samples were measured: bare silicon (5 μm thick) (black), NCF arrays with lattice constants of

600nm ($r_1$ = 69 nm, $r_2$ = 300 nm, green), 800nm ($r_1$ = 170 nm, $r_2$ = 400 nm, blue), and 1μm ($r_1$ = 273 nm, $r_2$ = 500 nm, red). All the window membranes consist of 3.5 μm of ordered Si NCF arrays, 1.5 μm of planar Si layer underneath and 2 μm of the SOI buried oxide.